ORIGINAL ARTICLE

Journal Section

Impact of Sky Temperature Models on Photovoltaic Panel Energy Yield Estimation

Javier Solano[1] | Zhixue Zheng[2] | Michel Aillerie[3] | Rémy Claverie[4]

[1]EIFER – European Institute for Energy Research. Emmy-Noether-Straße 11 76131 Karlsruhe, Germany

[2]Université Marie et Louis Pasteur, UTBM, CNRS, institut FEMTO-ST, FCLAB, F-90000, Belfort, France

[3]Université de Lorraine & CentraleSupélec, LMOPS, F-57070 Metz, France

[4]Cerema Est, TEAM Research Group, F-54510 Tomblaine, France

Correspondence
Michel Aillerie
Email: michel.aillerie@univ-lorraine.fr

Funding information
This work is in the framework of the Photovoltaic and green ROOF (PROOF) project funded by the French Research Agency - ANR Grant number no ANR-19-CE22-008.

The efficiency of photovoltaic (PV) panels, determined by irradiance and operating temperature, depends on thermal interaction with the environment. Solar radiation is the main thermal input, while energy conversion, convection, and radiation fluxes are the primary heat dissipation mechanisms. Radiation fluxes are based on boundary temperatures, such as ground and sky temperature, making accurate sky temperature estimation essential. However, despite its importance, there is limited work comparing the available models, which are often either very simplified or highly complex and adapted to specific geographic conditions.

This article examines five sky temperature models and their impact on estimating the operating temperatures of photovoltaic panels. Experimental validation shows that variations in sky temperature estimates lead to significant differences in panel operating temperatures. Although the effect on energy generation estimates is smaller, the findings highlight the importance of accurate sky temperature models for better PV performance predictions. This study provides a basis for improving PV energy yield forecasts through enhanced sky temperature modeling.

KEYWORDS

Photovoltaic panels, thermal modelling, sky temperature, energy estimation

Graphical Table of Contents

Impact of Sky Temperature Models on Photovoltaic Panel Energy Yield Estimation

Javier Solano, Zhixue Zheng, Michel Aillerie*, Rémy Claverie

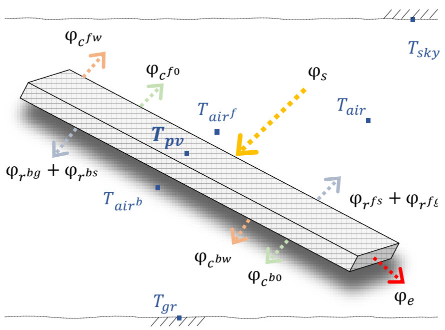

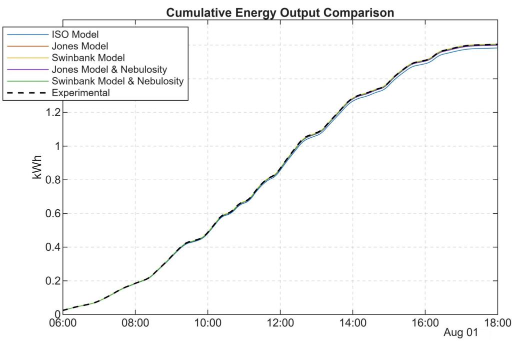

Five widely used sky temperature models were compared for photovoltaic thermal simulations: ISO ambient model, Jones model, Swinbank model, Jones with cloudiness, and Swinbank with cloudiness.

For module temperature prediction, the highest accuracy was achieved by the Jones with cloudiness and Swinbank with cloudiness models, whereas the ISO ambient model produced the weakest results. For energy yield estimation, differences between models were relatively small and no clear superior approach was identified. Therefore, simpler Jones or Swinbank formulations remain practical options when the objective is energy prediction, with limited impact on final yield estimates.

1 | INTRODUCTION

The performance of photovoltaic (PV) panels is strongly influenced by environmental factors such as solar irradiance, ambient temperature, and wind conditions. The fraction of solar radiation not converted into electricity is dissipated as heat, increasing the operating temperature of the panels and reducing their efficiency. The temperature of PV cells results from the interaction of heat transfer mechanisms, including conduction, convection, and radiation, together with external environmental conditions. Accurate modeling of these processes is essential for predicting PV performance under varying operating conditions.

A key aspect of thermal modeling is the proper representation of boundary conditions, particularly ground and sky temperatures, which directly affect radiative heat fluxes. Sky temperature plays a major role in determining radiative losses. Despite the availability of multiple models to estimate sky temperature, no clear consensus exists. This lack of agreement can lead to significant discrepancies in the predicted operating temperature of PV panels.

Sky temperature models are commonly used to estimate radiative heat exchanges in applications such as building energy analysis and photovoltaic (PV) systems. Numerous models have been developed, but significant discrepancies persist among them. Most of these models were originally developed and validated for the building sector, where their application has received considerable attention in the literature. In contrast, studies focused on the selection of appropriate models for PV systems remain limited. Many photovoltaic studies include one or two sky temperature models but adopt them without a structured justification or comparison. This may be because the main differences between models are most evident during nighttime hours when PV panels do not generate energy. However, in applications such as building climate control or pool heating, these models are scrutinized more thoroughly due to their continuous impact on energy performance.

In evaluating sky temperature models, this study focuses on formulations recognized for their historical relevance, practical applicability, and frequent use. Models noted for their simplicity and ease of use have been selected, despite potential shortcomings in complex environmental scenarios typical for PV systems. The objective is to identify which models most accurately reproduce real operating temperatures of PV panels, thereby improving energy yield prediction. This effort directly supports the broader objective of optimizing PV system designs and energy management practices, making the findings relevant to the improvement of renewable energy technologies.

This study evaluates five widely used sky temperature models to assess their accuracy in estimating PV panel temperatures and their impact on energy production predictions. These models were selected based on their prominence in the literature and relevance to PV energy studies. The analysis combines experimental validation with model comparison to identify the most reliable approach for improving thermal predictions. Although the direct impact on energy yield estimates may be moderate, accurate sky temperature modeling enhances the reliability of thermal models and overall PV system performance assessments. The findings of this study aim to enhance PV thermal modeling techniques, improve energy yield predictions, and advance methods for evaluating PV performance under real-world conditions.

1.1 | Literature Review

Accurate modeling of radiative heat exchanges, influenced by sky temperature, plays a crucial role in many applications. Historically, these efforts have been primarily focused on the building sector, where thermal performance assessments depend on precise sky temperature modeling. Many modeling studies on photovoltaic panels discussed below incorporate one sky temperature model or another to estimate radiative heat exchanges. However, limited research addresses how to select among available sky temperature models.

One of the earliest widely recognized models was proposed by [1], which estimated long-wave radiation under clear skies based solely on ambient temperature. This model has since become a reference for radiative exchange calculations, particularly in applications requiring simplicity and broad applicability. The Swinbank model has been employed in studies such as [2, 3, 4, 5].

Measuring or estimating sky temperature is complex and rarely accessible, leading some authors to use ambient temperature as a proxy for sky temperature [6, 7, 8, 9, 10]. However, as it is widely accepted that sky temperature is lower than ambient temperature, particularly under clear sky conditions, several studies, including those by the International Organization for Standardization (ISO), adopted simplified approaches to sky temperature estimation, as outlined in ISO 6946:2017 [11]. The model proposed by [12] assumes that the sky temperature has an offset of 20°C, as shown in Equation 21. This model has been used in studies such as [13, 14, 15, 16, 17]. Some authors such as [18] and [19] use adaptations of the Swinbank or Jones models to account for cloud conditions, as presented in Section 2.6.4.

Several other empirical models have been proposed, including the model presented in [20], which has been applied in studies such as [21]. Other models, such as the one proposed by [22], use advanced instrumentation to estimate sky temperature. The model proposed by [23] is used in PV panels and is also implemented in the TRNSYS software and in studies such as [24]. This model adds an additional layer of complexity because it includes dew temperature and was originally developed for US weather conditions, which are themselves geographically diverse and seasonally variable. From a macroscopic perspective, it is challenging to justify the use of highly complex models to estimate the temperature or energy production of PV panels. The primary reason to prioritize simple models is the inherent uncertainty in model inputs. Irradiance, wind, and temperature profiles are neither spatially uniform nor fully predictable over extended periods. For example, the research presented in [18] concludes that, based on long-term weather forecasts, no advantages are observed in developing dynamic models. These findings highlight the importance of selecting models that balance accuracy and practicality. For this study, we selected widely adopted models requiring minimal and readily available input data, such as ambient temperature.

Some studies, such as [25, 26, 27], and more recently [28, 29, 30], analyze the effect of different sky temperature models on estimating building heat losses. However, we did not identify references comparing the effect of sky temperature models on the temperature or energy production modeling of photovoltaic panels.

Recent studies continue to confirm the importance of accurate thermal modeling for photovoltaic systems and the sensitivity of predicted performance to model formulation and environmental inputs. Pereira [31] emphasizes that different thermal formulations can lead to significant differences in predicted PV behavior, highlighting the need for systematic comparison of available approaches. Liu [32] proposes an updated empirical temperature model that incorporates radiative effects while maintaining low complexity, illustrating the ongoing development of simplified predictive methods. Ahmad et al. [33] provide a comprehensive review of thermo-electrical PV models and identify the need for improved representation of physical heat transfer mechanisms. Driesse [34] shows that including radiative exchange with the sky can improve the accuracy of commonly used PV temperature models.

Other recent works further demonstrate the influence of environmental conditions on PV temperature and energy production. Aoun [35] develops a methodology for predicting PV module temperature using measured and estimated meteorological data, showing the sensitivity of results to input quality. Hassan [36] analyzes the impact of environmental parameters on PV energy extraction and confirms the strong influence of module temperature on system performance. Detailed thermal formulations based on coupled conduction, convection, and radiation mechanisms continue to be proposed to improve temperature prediction accuracy [37]. Pereira [38] combines thermal modeling with forecasting approaches, underlining the importance of reliable temperature estimation for power prediction. Li [39] examines the effect of environmental variability, including cloud cover, on PV performance under real operating conditions.

Several studies have also compared PV module temperature models for energy yield estimation. Correa-Betanzo et al. [40] evaluate seasonal energy yield using different module temperature formulations based on ambient temperature, irradiance, and wind speed, without explicitly addressing sky temperature model selection. In parallel, sky temperature estimation methods continue to be investigated extensively in building simulation studies [41], where longwave radiative exchange is a central modeling component.

This study evaluates the performance of five sky temperature models to estimate the temperature of the PV panel: (1) the basic model adopted by the International Organization for Standardization [11]; (2) a similar model with an offset proposed by [12]; (3) the model proposed by [1]; and (4,5) two variations that account for cloudiness, as presented in Section 2.6.

Although the studies discussed in this section provide important advances in PV thermal modeling, environmental analysis, and energy yield prediction, a specific gap remains regarding the role of sky temperature formulation in photovoltaic applications. The reviewed literature does not provide a systematic comparison of multiple sky temperature models within a unified PV thermal framework combined with extended experimental validation under real operating conditions. The present study addresses this gap by systematically comparing these models and quantifying their influence on PV module temperature prediction and associated energy yield estimates.

1.2 | Structure of the paper

The paper is structured as follows. Section 2 discusses the modeling of PV panels. Section 3 presents the model calibration. Section 4 presents, compares, and discusses simulation and experimental results. Finally, Section 5 concludes with the findings and outlines directions for future research.

2 | PV PANELS AND OPERATING ENVIRONMENT

This section presents the thermal modeling framework of the PV system. Section 2.1 details the global model, including its inputs and outputs. Sections 2.2 and 2.3 focus on convection and radiation fluxes. The boundary condition associated with ground temperature is introduced in Section 2.4. Section 2.5 presents the local air temperatures surrounding the PV panel. Finally, Section 2.6 presents the five sky temperature models compared in this paper.

2.1 | Global Thermal Model

The power generated by a PV panel is mainly influenced by solar irradiance and the operating temperature of the panel. Solar irradiance is treated as an external input to the model. As described by Equation 1, the panel operating temperature, T_{pv} $(^\circ C)$, is obtained from an energy balance including heat gains, heat losses, and thermal capacitance. The thermal capacity of the panel is denoted by C_{th} $\left(J \cdot {}^\circ C^{-1} \cdot m^{-2}\right)$.

$$\varphi_s - \varphi_e - \varphi_r - \varphi_c - C_{th}\frac{dT_{pv}}{dt} = 0 \tag{1}$$

The principal source of heat is the solar flux, φ_s. Heat losses include radiative fluxes, φ_r, convective fluxes, φ_c, and the fraction converted into electricity, φ_e, which represents energy removed from the thermal balance.

Figure 1 depicts the heat flux balance, illustrating the various components of radiation and convection fluxes discussed further in this section.

Adopting a macroscopic heat flux balance model offers a viable compromise between computational cost and the validation of available data. The complexity of this model can match that of its subsystem models. For simplification, the following assumptions are made in this work:

- The temperature across the PV panel is assumed to be uniform.
- This temperature is measured at the rear surface of the panel.
- The temperature gradient between the panel's front and rear is considered constant.
- The impact of dust accumulation on the surface of the panel is overlooked.
- The impact of shading from surrounding structures is not within the scope of this work.

Internal conductive temperature gradients through the thin laminated PV module are assumed negligible. Therefore, the panel is modeled as a lumped thermal mass with uniform temperature. This assumption is consistent with prior works such as [3] and [37].

To determine the heat losses associated with the conversion of electricity per unit of area, φ_e, Equation 2 is used. Equation 3 is used to compute the power generated by the PV panel, P_{pv} (W). Parameters such as the PV panel area, A_{pv} (m^2), its efficiency, η_{pv} (dimensionless), the thermal coefficient, β $(^\circ C^{-1})$, and the thermal capacity, C_{th}, can be derived from the panel's datasheet. This model does not account for the degradation process that may reduce

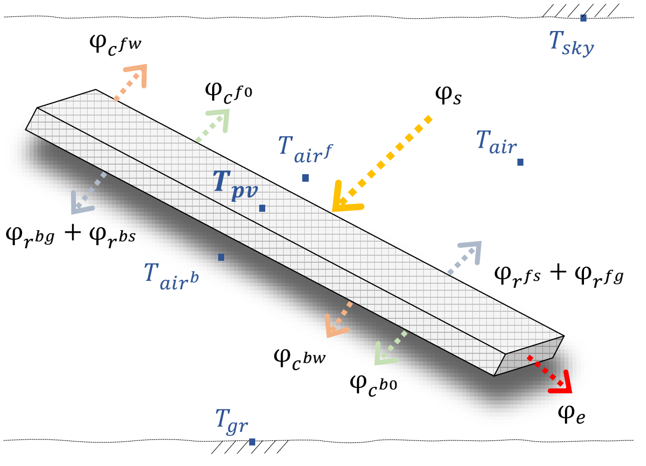

FIGURE 1 Balance of heat flows at the PV panel.

efficiency and assumes these parameters remain constant.

$$\varphi_e = \eta_{pv} \cdot \varphi_s \left(1 - \beta \left(T_{pv} - 25\right)\right) \tag{2}$$

$$P_{pv} = \varphi_e \cdot A_{pv} \tag{3}$$

2.2 | Convection Fluxes

The PV panel exchanges heat with its surroundings through convection φ_c. These exchanges occur on both the front and the back surfaces of the panel, influenced by the air temperature immediately surrounding the panel at its back, ${T_{air}}^b$, and at its front, ${T_{air}}^f$. The convective fluxes at the back, ${\varphi_c}^b$, and at the front, ${\varphi_c}^f$, as defined in Equation 4, depend on the convective heat transfer coefficients h_b and h_f $(W \cdot K^{-1} \cdot m^{-2})$, detailed in Equations 5 and 6.

$$\varphi_c = {\varphi_c}^f + {\varphi_c}^b \tag{4}$$

$${\varphi_c}^f = h^f \left(T_{pv} - {T_{air}}^f\right) \tag{5}$$

$${\varphi_c}^b = h^b \left(T_{pv} - {T_{air}}^b\right) \tag{6}$$

The convective heat transfer coefficients are influenced by various factors, including geographical position, panel geometry, and its inclination and orientation [16]. To account for the effect of wind on forced convection, most studies model a linear dependency on wind speed v_w $(m \cdot s^{-1})$. Thus, the convective heat transfer coefficient comprises a constant component and a wind speed-dependent component, as shown in Equations 7 and 8.

$$h^f = h^{f0} + h^{fw} \cdot v_w \tag{7}$$

$$h^b = h^{b0} + h^{bw} \cdot v_w \tag{8}$$

Defining the values of these coefficients is challenging, with many authors suggesting empirical values [16, 42, 19, 43, 5]. The calibration of these model parameters is discussed in Section 3.

Figure 2 illustrates the interconnections among the different components (subsystems), using arrows to indicate the flow of information between them. The corresponding inputs and outputs are described in the following subsections.

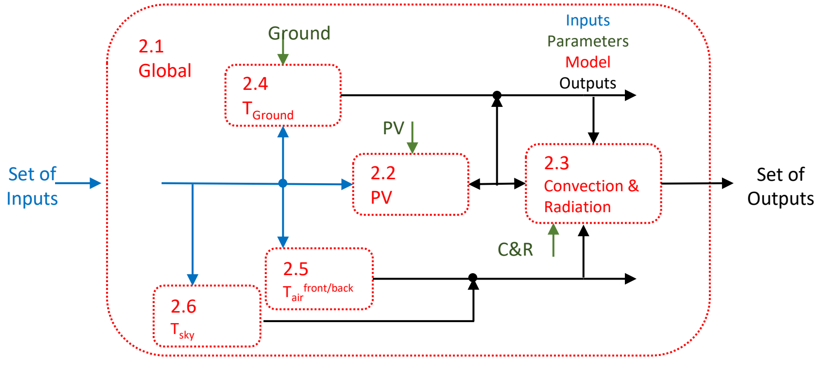

FIGURE 2 Systematic study of the PV system.

2.3 | Radiative Fluxes

The PV panel also exchanges heat with its environment through radiation φ_r, occurring at both the panel's front and back surfaces. These radiative fluxes are contingent upon boundary conditions, such as the ground, T_{gr}, and sky, T_{sky}, temperatures. Equations 9 through 13 describe the four modes of radiative exchange: from the back surface to the ground, $\varphi_{r_{bg}}$, and to the sky, $\varphi_{r_{bs}}$; and from the front surface to the ground, $\varphi_{r_{fg}}$, and to the sky, $\varphi_{r_{fs}}$. Here, ε_{pv} is the panel's emittance (dimensionless), and σ represents the Stefan-Boltzmann constant $5.67 \cdot 10^{-8}(W \cdot m^{-2} \cdot K^{-4})$. The factors F_{bs}, F_{fs}, F_{bg}, and F_{fg} are dimensionless view factors for the panel's back and front surfaces in relation to the sky and ground. In the Stefan-Boltzmann exchange Equations following Equation 9, T_{pv}, T_{sky}, and T_{gr} are expressed in Kelvin.

$$\varphi_r = \varphi_{r_{fs}} + \varphi_{r_{fg}} + \varphi_{r_{bs}} + \varphi_{r_{bg}} \tag{9}$$

$$\varphi_{r_{bs}} = \varepsilon_{pv} \cdot \sigma \cdot F_{bs} \cdot \left({T_{pv}}^4 - {T_{sky}}^4\right) \tag{10}$$

$$\varphi_{r_{fs}} = \varepsilon_{pv} \cdot \sigma \cdot F_{fs} \cdot \left({T_{pv}}^4 - {T_{sky}}^4\right) \tag{11}$$

$$\varphi_{r_{bg}} = \varepsilon_{pv} \cdot \sigma \cdot F_{bg} \cdot \left({T_{pv}}^4 - {T_{gr}}^4\right) \tag{12}$$

$$\varphi_{rfg} = \varepsilon_{pv} \cdot \sigma \cdot F_{fg} \cdot \left({T_{pv}}^4 - {T_{gr}}^4 \right) \tag{13}$$

The view factors are defined in Equations 14 to 17. Here, δ is the inclination angle in degrees (°) of the PV panels.

$$F_{bs} = \frac{1}{2} \cdot (1 + \cos\delta) \tag{14}$$

$$F_{bg} = \frac{1}{2} \cdot (1 - \cos\delta) \tag{15}$$

$$F_{fs} = \frac{1}{2} \cdot (1 + \cos(180 - \delta)) \tag{16}$$

$$F_{fg} = \frac{1}{2} \cdot (1 - \cos(180 - \delta)) \tag{17}$$

2.4 | Ground Temperature

Ground temperature directly affects the local air temperature near the rear side of the PV panel and consequently influences its back surface temperature. It is governed by factors such as thermal conductivity, solar irradiance absorption, and heat exchange with the surrounding environment. For ground-mounted systems, relevant parameters include soil type, moisture content, and surface cover, whereas for rooftop systems, the thermal properties of roofing materials become significant.

In this study, ground temperature was directly measured. This choice was made because the primary objective of the paper is to evaluate the influence of sky temperature on PV panel performance. Using measured ground temperature allows the incorporation of real operating data while reducing the uncertainty associated with introducing an additional ground temperature model.

2.5 | Local Air Temperature Models

The air temperature in the immediate vicinity of the panel primarily depends on the local ambient and ground temperature.

The air temperature at the panel's front, ${T_{air}}^f$, is often equated to the local ambient temperature, T_{amb}, as indicated in Equation 18.

$${T_{air}}^f = T_{amb} \tag{18}$$

The ground significantly influences the local air temperature near the panel's back, ${T_{air}}^b$. This temperature is expected to lie between the air and ground temperatures. A modulation factor, α, is introduced to estimate the temperature at the panel's rear, as shown in Equation 19. For $\alpha = 0$, the temperature at the panel's back equals the ambient temperature, and for $\alpha = 1$, it matches the ground temperature. This dynamic parameter is influenced by factors such as ground type and the panel's relative height.

$${T_{air}}^b = (1 - \alpha)T_{amb} + \alpha T_{gr} \tag{19}$$

2.6 | Sky Temperature Models

This study assess the performance of the following five models of sky temperature: 1- the basic model adopted by the International Organization for Standardization [11] as proposed in Equation 20; 2- a similar model with an offset proposed by [12] and presented in Equation 21; 3- the model widely used in PV panels presented by [1] and defined in Equation 22, and finally; 4, 5- their variations accounting for cloudiness as presented in Equations 23 and 24.

2.6.1 | Model 1: Ambient Temperature - ISO model

The initial model, outlined in Equation 20, equates sky temperature directly to ambient air temperature, offering a simplified approach for sky temperature estimation.

$$T_{sky_1} = T_{air} \tag{20}$$

2.6.2 | Model 2: Ambient Temperature with Offset - Jones model

In practical terms, the upper bound on sky temperature is the ambient temperature, and its lower bound is approximately 30°C below ambient. The model proposed by [12] considers that the sky temperature has an offset of 20°C, as presented in Equation 21.

$$T_{sky_2} = T_{air} - 20 \tag{21}$$

2.6.3 | Model 3: Nonlinear Sky Temperature Dependence - Swinbank Model

One of the most widely used models of sky temperature was introduced by [1], as shown in Equation 22.

$$T_{sky_3} = 0.0552 T_{air}^{1.5} \tag{22}$$

2.6.4 | Model 4 and Model 5: Sky Temperature Model including Additional Weather Considerations

The previous models only consider the ambient temperature as input. However, additional weather variables such as cloud conditions or dew temperature play a crucial role in determining sky temperature. The parameter γ in the following equations indicates the cloud cover factor, ranging from 0 oktas (clear sky) to 8 oktas (overcast). The first model is a variation of the Jones model as presented in Equation 23.

$$T_{sky_4} = \gamma(T_{air} - 20) + (1 - \gamma)T_{air} \tag{23}$$

The second model is a variation of the Swinbank model as presented in Equation 24.

$$T_{sky_5} = \gamma(0.0552 {T_{air}}^{1.5}) + (1 - \gamma)T_{air} \tag{24}$$

3 | SKY TEMPERATURE MODELS' CALIBRATION

Calibration of the models is required for ensuring that simulation results closely match experimental data. While some parameters are straightforward to define due to their geometric nature or availability on the PV panel datasheet, others, like the radiation convection coefficients h_b and h_f require a deeper approach for accurate determination.

This section outlines the methodology employed to calibrate these parameters. By optimizing the model to reflect empirical observations, we aim to enhance its predictive accuracy and reliability across various operational conditions.

3.1 | Optimization Problem

The calibration process is formulated as an optimization problem, where the objective is to minimize the difference between measured and simulated PV panel temperatures. The problem is defined as follows:

Minimize $J\left(\widehat{r}\right)$ subject to $\underline{\widehat{r}} < \widehat{r} < \widehat{\widehat{r}}$, where

$$J\left(\widehat{r}\right) = \int_{t_i}^{t_f} \left(T_{pv}^{meas} - T_{pv}^{sim}\left(\widehat{r}, \widehat{W(t)}\right)\right)^2 dt.$$

Here, $\widehat{r}$ represents the set of model parameters, and $\widehat{W(t)}$ denotes the set of model inputs. The parameter search space is constrained by $\underline{\widehat{r}}$ and $\widehat{\widehat{r}}$.

3.2 | Model Parameters

Parameters are categorized into two sets for clarity:

- The first set includes the view factors, P_{nom}, β, C_{th}, and A_{pvp}, directly sourced from the PV panel datasheet or from anaytical expressions.
- The second set comprises α, h_b and h_f, which are less straightforward and require calibration.

Inputs such as q_s and T_{air} are derived from synthetic data, in-field measurements, or additional models.

3.3 | Parameter Identification

An identification algorithm is proposed that utilizes inputs, such as φ_s, T_{air}, and C_{th}, along with P_{nom}, β, and A_{pvp} to determine the values of α, h_b, and h_f. This algorithm, visualized in Figure 3, leverages genetic algorithms, simulated annealing, or particle swarm optimization (PSO) for parameter estimation, as also suggested in related research [44, 45].

The task involves a complicated optimization problem, which includes comparing several models with distinct sets of optimal parameters. Due to the strong interdependence of these aspects, a single, consistent approach for model comparison has been defined. Parameter values are set to the average obtained from each sky temperature model optimal parameters. These fixed values are then utilized to compare the sky models under identical conditions. In the subsequent step, optimization is eschewed in favor of straightforward simulation.

The optimization algorithm was implemented in MATLAB Simulink. The evaluated optimizers included genetic algorithms, PSO, fmincon, simulated annealing, and a mixed approach combining genetic algorithms with fmincon. Based on the cost function defined in Section 3.1, PSO consistently emerged as the most effective optimization

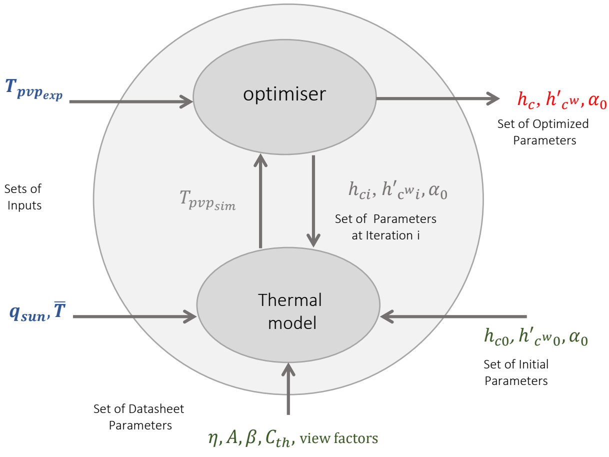

FIGURE 3 Parameter identification algorithm.

method. Consequently, the results ultimately retained and presented are those obtained with PSO. Table 1 consolidates the simulation parameters derived from datasheets, as well as those estimated using analytical models and identification algorithms.

Model comparison was performed using deterministic error indicators, namely MSE, MAE, and ME, computed over the same experimental dataset for all tested formulations. Because each model was evaluated under identical boundary conditions and with the same measurement series, these metrics provide a direct and consistent basis for relative performance assessment. Given the deterministic nature of the comparison and the use of identical time series for all models, statistical hypothesis testing was not pursued.

The identified parameters result from an optimization process minimizing the deviation between simulated and measured module temperatures. Their influence is therefore inherently reflected in the final objective function values and associated prediction errors. Although a dedicated sensitivity analysis of α, h_b, h_f, and sky temperature offsets was not included in the present study, such an extension would be valuable for assessing parameter robustness and transferability under different climatic conditions.

TABLE 1 Parameters for PVP System

Parameter	Symbol	Value	Units
Thermal Coefficient	β	0.004	$[1/K]$
Nominal Power	P_{nom}	310	$[W]$
Surface Area	A	1.6434	$[m^2]$
Thermal Capacity	C_{th}	9113	$[J/K/m^2]$
Panel inclination angle	δ	30	$[°]$
Convective Heat Transfer Coefficient	h_0	0.444	$[K \times m^2/W]$
Wind Heat Transfer Coefficient	h_w	0.699	$[K \times m^2/W]$
Modulation factor	α	0.89	-

4 | EXPERIMENTAL PLATEFORM AND MEASUREMENTS

In the framework of the French ANR PROOF project, a research platform was designed and implemented on the Cerema building roofs located in Nancy district, in the northeastern of France as illustrated in Figure 4. The site is equipped with a complete meteorological station, including global irradiance meters. The instruments measuring pressure, relative humidity, wind speed, and wind direction comply with the standards set by the French meteorological agency Meteo France located close the platform while the remaining instruments are managed by the Cerema. All data, including global irradiance, pressure, relative humidity, wind speed, and wind direction, are collected and recorded at one minute intervals.

FIGURE 4 Experimental platform.

The PV module was installed facing south with a tilt angle of 30°, consistent with the experimental configuration and representative of installations commonly used to favor summer energy production in eastern France. Variations in tilt angle would modify the incident irradiance and therefore the thermal balance of the module, but would not alter the structure of the proposed thermal model. The PV module was connected to a maximum power point tracking (MPPT) controller and an Enphase microinverter for power conversion, which also provided measurements of generated and consumed energy.

Nine PT1000 platinum resistance temperature detectors (RTDs) were mounted on the rear surface of the module to monitor the spatial temperature distribution. The panel surface was divided into nine sections arranged in a three by three grid, with one RTD positioned at the center of each section, including one located at the geometric center of the module, as described in [46] and in [47].

This section presents, first, the experimental data in Section 4.1. Section 4.2 presents, the comparison of the temperatures obtained via the various existing models.

4.1 | Experimental Data

Experimental data were collected from August to December 2021, with measurements taken every minute. This period covers a wide range of irradiance and ambient temperature conditions suitable for comparative model assessment. The objective of the study is to compare different modeling approaches under identical inputs rather than to perform a full annual validation. Since the analysis is based on time invariant heat transfer relationships, the use of the 2021 dataset does not affect the comparative validity of the results. All relevant variables were continuously monitored throughout the measurement period, ensuring consistency and completeness of the dataset.

The results of this study are based on measurements obtained at a single site in northeastern France. However, the objective of this work is not to provide site specific calibration, but to compare modeling approaches under identical conditions. The comparison framework is independent of the site and can be applied to other climates, provided that appropriate local input data are available. The relative behavior of the models is primarily driven by irradiance levels, ambient temperature, and longwave radiation conditions, which may differ in arid, tropical, or high altitude environments. The quantitative performance of the models may vary under different climatic conditions and should therefore be reassessed using local data.

Figure 5 illustrates the experimental measurements considered in this study. From top to bottom, the plots present wind speed, nebulosity, global irradiance, ambient temperature, ground temperature, mean rear module temperature, and generated power.

Nebulosity is included because several sky temperature formulations reported in the literature use cloud cover as an input variable for estimating longwave radiative exchange as shown in Section 2. The available nebulosity data were obtained from the nearby public Météo France weather station and were not continuously reported, which explains the gaps visible in the measurement series. This limited availability constitutes an important practical constraint, since the use of nebulosity may require dedicated instrumentation or external meteorological databases. The results further indicate that introducing this parameter increases model complexity without providing a significant improvement in prediction accuracy.

4.2 | Sky Temperature Models' Comparison

The dataset was segmented into three distinct subsets: the first encompassing data from a single summer day, the second spanning observations over a ten-day period in autumn, and the third encapsulating data collected from August to December 2021, spanning four months. Within each dataset, simulations were conducted for the five proposed models.

As a reminder, the models are as follows:

- Model 1: $T_{sky_1} = T_{air}$
- Model 2: $T_{sky_2} = T_{air} - 20$
- Model 3: $T_{sky_3} = 0.0552T_{air}^{1.5}$
- Model 4: $T_{sky_4} = \gamma(T_{air} - 20) + (1 - \gamma)T_{air}$
- Model 5: $T_{sky_5} = \gamma(0.0552{T_{air}}^{1.5}) + (1 - \gamma)T_{air}$

The outcomes of these simulations are summarized in Table 2. The best results obtained for each dataset are

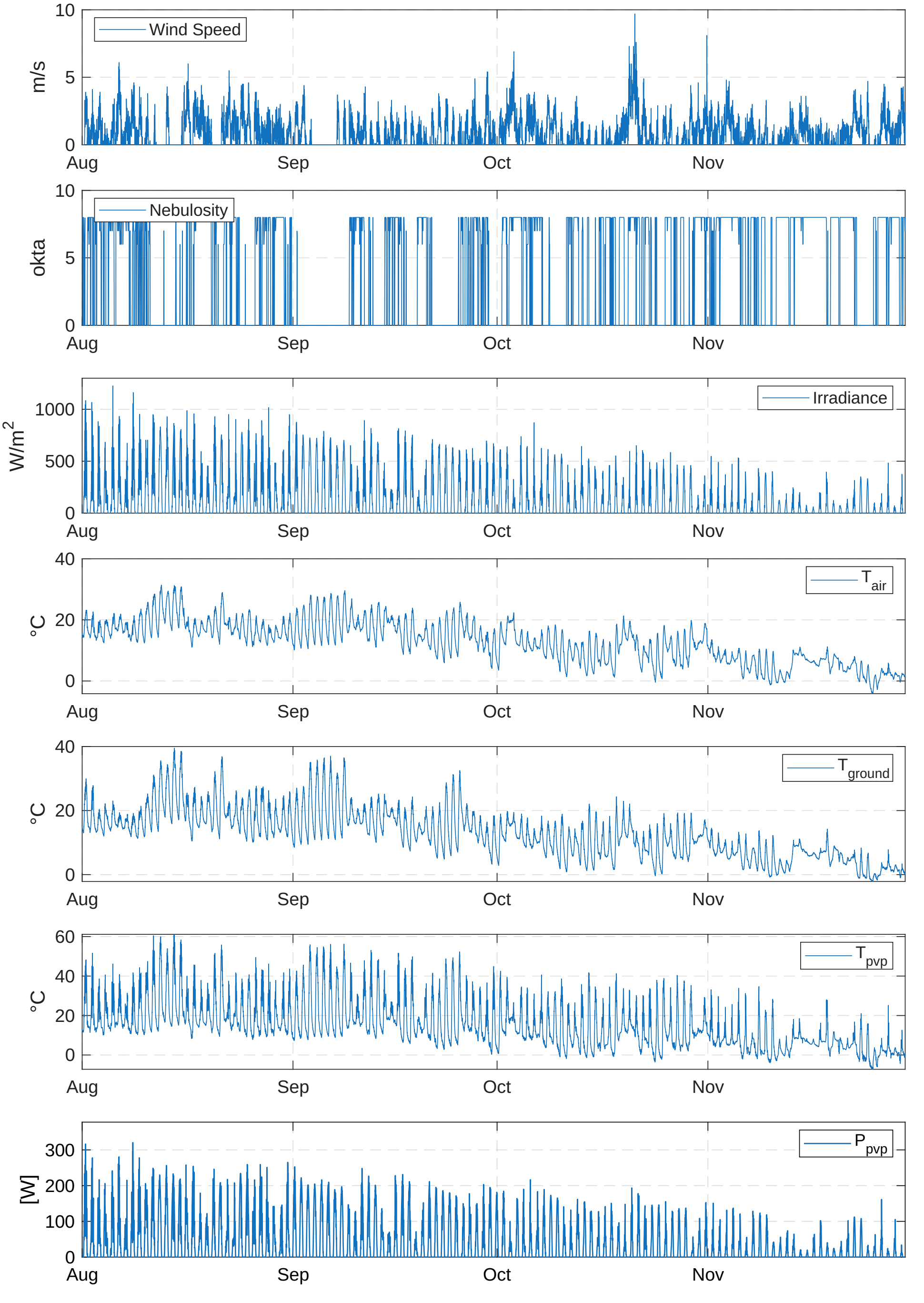

FIGURE 5 Experimental measurements.

visually depicted in Figure 6.

TABLE 2 Evaluation metrics for different datasets and T_{sky} models.

Data Set	T_{sky} model	Metrics		
		MSE	MAE	ME
1	1	12.15	2.88	-2.28
	2	8.98	2.19	1.35
	3	**8.00**	**2.03**	0.85
	4	8.26	2.07	**-0.34**
	5	8.03	2.10	-0.68
2	1	10.82	2.89	-2.70
	2	14.31	2.91	2.84
	3	14.01	2.91	2.86
	4	8.67	**1.81**	**0.98**
	5	**8.46**	1.82	1.01
3	1	11.78	2.94	-2.33
	2	10.12	2.57	2.28
	3	9.57	2.49	2.10
	4	6.63	1.72	0.54
	5	**6.20**	**1.67**	**0.40**

Models 4 and 5, considering the nebulosity, emerge as the top performers with the lowest average Mean Squared Error (MSE) and Mean Absolute Error (MAE). Furthermore, in terms of Mean Error (ME), Model 4 demonstrates the least bias, closely followed by Model 2. Overall, Model 4 stands out as the best-performing model, demonstrating the lowest MSE, competitive MAE, and relatively low bias. Model 5 also performs well, particularly in terms of bias. Model 1 emerges as the worst performer among the compared models, displaying the highest average MSE, MAE, and significant negative bias.

To analyze the effect of temperature estimation errors using different models, energy generation during the designated time frames was simulated. The summarized results can be found in Table 3, and a comparison of the results obtained for each model over the entire 4-month period is illustrated in Figure 7. Here, models 4 and 5 continue to exhibit the best performance. Energy estimation errors are consistently below 1% for most cases compared to experimental values. The relative difference between the best and worst performing models is approximately 1%.

It's noteworthy that while considering nebulosity improved results in terms of temperature estimation, the difference, even if still present, is less significant and sometimes negligible in some datasets. Given the additional complexity and uncertainty associated with nebulosity data and the simulation process utilizing synthetic data, recommending a more complex model may not be prudent. In such cases, opting for models without nebulosity consideration could be more straigthforward without loss of accuracy. Additionally, the model where air temperature alone is considered consistently performs the worst and it is not recommended for use in this context.

5 | CONCLUSION

This study highlights the importance of the sky temperature formulation in the thermal modeling of photovoltaic panels and its influence on predicted module temperature and energy production. Five commonly used sky temperature models were implemented within the same physical framework and evaluated using several months of experimental measurements obtained under real operating conditions.

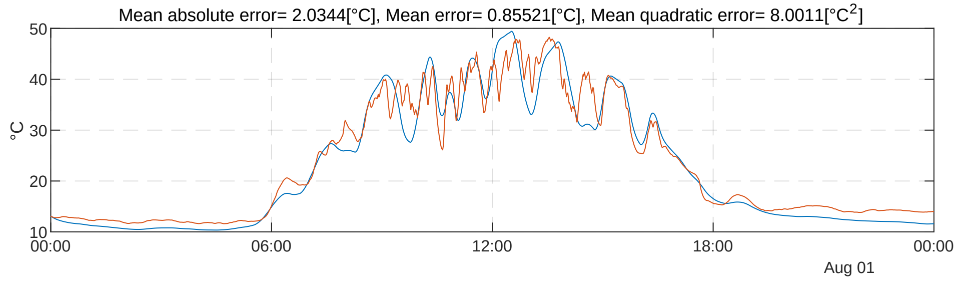

(a) Dataset 1 - one day in summer - Model 3.

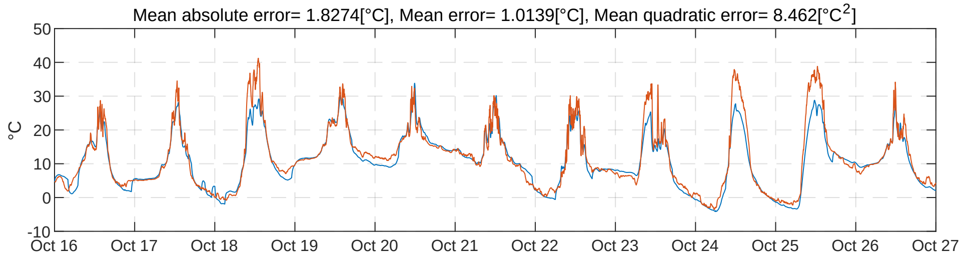

(b) Dataset 2 - ten days in October - Model 5.

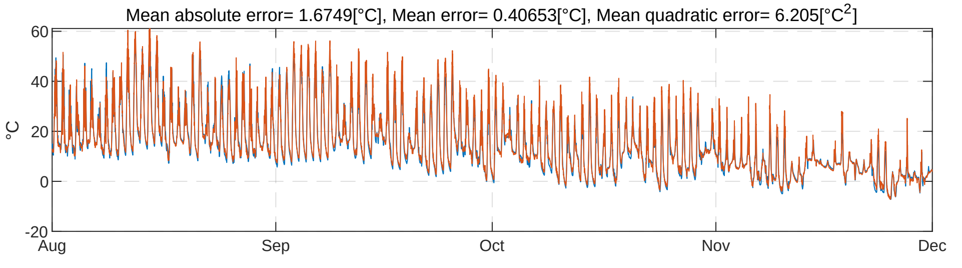

(c) Dataset 3 - four months in the year - Model 5.

FIGURE 6 Photovoltaic Panel Temperatures - Model Evaluation. Experimental data in red - Simulation data in blue.

The results show that the choice of sky temperature model is not negligible, since it directly affects the radiative heat exchange between the module and the sky. Models including nebulosity effects generally provided the best agreement with measured temperatures, while the simplest assumption consisting of equating sky temperature to ambient temperature produced the largest deviations. The observed differences remained moderate, reaching approximately 1% for temperature prediction and about 0.5% for estimated energy yield.

From a practical perspective, the most accurate formulations are not always the most suitable because some required inputs, especially nebulosity, are not systematically measured or may contain missing or uncertain values in publicly available meteorological databases. In addition, the inclusion of such variables increases model complexity without producing a clear advantage in energy estimation. For power and energy prediction, no formulation showed systematic superiority under all tested conditions.

The proposed comparison framework constitutes one of the main contributions of this work. Unlike previous studies focused mainly on empirical temperature laws or site specific calibrations, the present approach provides a

TABLE 3 Evaluation metrics for different datasets and Tsky models.

Data Set	Energy T Exp (kWh)	Energy T Model (kWh)	Error %
1	1.61	1.59	-1.33
		1.62	0.13
		1.61	-0.15
		1.61	-0.07
		1.61	-0.32
2	6.61	6.66	0.77
		6.75	2.15
		6.75	2.10
		6.70	1.39
		6.70	1.36
3	103.38	102.96	-0.41
		104.47	1.05
		104.23	0.83
		103.92	0.53
		103.74	0.35

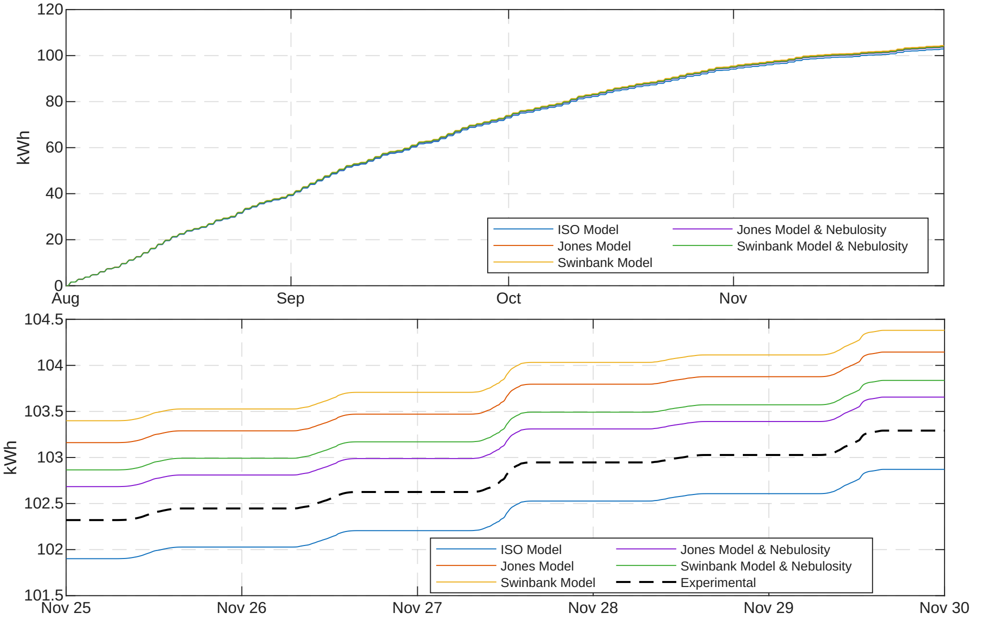

FIGURE 7 Total energy generation across a four month period (top), zoomed final days view (bottom)

consistent assessment of several sky temperature formulations within the same PV thermal model using identical inputs and extended outdoor measurements. This makes it possible to isolate the specific influence of the radiative boundary condition on model performance.

The results also indicate that simplified formulations may remain adequate when the objective is annual energy estimation or operational monitoring, whereas more detailed sky temperature models become more relevant when accurate module temperature prediction is required for thermal diagnostics, degradation studies, or detailed system simulations.

The present study is based on measurements from a single temperate site in northeastern France. Although the methodology is transferable to other locations, quantitative results may differ under arid, tropical, coastal, or high altitude climates where atmospheric emissivity and cloud behavior are different. Additional validation under contrasted climates would therefore be valuable.

Future work should extend the analysis to other climatic regions, include direct longwave radiation measurements when available, and investigate transient effects such as rainfall, condensation, or rapid cloud passages. The coupling of improved sky temperature estimation with forecasting tools and real time monitoring systems also represents a relevant perspective for enhanced PV performance prediction.

Declaration of Competing Interest

The authors declare no conflict of interest. The funders had no role in the design of the study; in the collection, analyses, or interpretation of data; in the writing of the manuscript, or in the decision to publish the results.

| Credit authorship contribution statement

J. Solano: Investigation, Formal analysis, Visualization, Methodology, Validation, Writing - Original draft & Final review. Z. Zheng: Investigation, Methodology, Validation, & Writing - Review. M. Aillerie: Conceptualization, Funding acquisition, Supervision, Investigation, Validation, Writing - Review, & Editing. R. Claverie: Resource, Conceptualization, Funding acquisition, Supervision, Validation, & Review.

References

[1] Swinbank WC. Long-wave radiation from clear skies. Quarterly Journal of the Royal Meteorological Society 1963;89(381):339–348.

[2] Yaman K, Arslan G. A detailed mathematical model and experimental validation for coupled thermal and electrical performance of a photovoltaic (PV) module. Applied Thermal Engineering 2021;195(June).

[3] Aly SP, Ahzi S, Barth N. Effect of physical and environmental factors on the performance of a photovoltaic panel. Solar Energy Materials and Solar Cells 2019;200(May):109948.

[4] Notton G, Cristofari C, Mattei M, Poggi P. Modelling of a double-glass photovoltaic module using finite differences. Applied Thermal Engineering 2005;25(17-18):2854–2877.

[5] Kaplani E, Kaplanis S. Thermal modelling and experimental assessment of the dependence of PV module temperature on wind velocity and direction, module orientation and inclination. Solar Energy 2014;107:443–460.

[6] Royne A, Dey CJ, Mills DR. Cooling of photovoltaic cells under concentrated illumination: a critical review. Solar energy materials and solar cells 2005;86(4):451–483.

[7] Hassanian R, Riedel M, Helgadottir A, Yeganeh N, Unnthorsson R. Implicit Equation for Photovoltaic Module Temperature and Efficiency via Heat Transfer Computational Model. Thermo 2022;2(1):39–55.

[8] Skoplaki E, Palyvos JA. On the temperature dependence of photovoltaic module electrical performance: A review of efficiency/power correlations. Solar Energy 2009 5;83(5):614–624.

[9] Lee Y, Tay AAO. Finite element thermal analysis of a solar photovoltaic module. Energy Procedia 2012;15:413–420.

[10] Zhou J, Yi Q, Wang Y, Ye Z. Temperature distribution of photovoltaic module based on finite element simulation. Solar Energy 2015;111:97–103.

[11] for Standardization IO. ISO 6946: 2017-Building components and building elements-Thermal resistance and thermal transmittance. Int Organ Stand Geneva, Switz 2017;.

[12] Jones AD, Underwood CP. A thermal model for photovoltaic systems. Fuel and Energy Abstracts 2002;43(3):199.

[13] Neises TW, Klein SA, Reindl DT. Development of a thermal model for photovoltaic modules and analysis of NOCT guidelines. Ecological Engineering 2012 2;134:1–7.

[14] Aly SP, Ahzi S, Barth N, Abdallah A. Using energy balance method to study the thermal behavior of PV panels under time-varying field conditions. Energy Conversion and Management 2018;175(July):246–262.

[15] Usama Siddiqui M, Arif AFM, Kelley L, Dubowsky S. Three-dimensional thermal modeling of a photovoltaic module under varying conditions. Solar Energy 2012;86(9):2620–2631.

[16] Torres-Lobera D, Valkealahti S. Inclusive dynamic thermal and electric simulation model of solar PV systems under varying atmospheric conditions. Solar Energy 2014;105:632–647.

[17] Hoang P, Bourdin V, Liu Q, Caruso G, Archambault V. Coupling optical and thermal models to accurately predict PV panel electricity production. Solar Energy Materials and Solar Cells 2014;125:325–338.

[18] Migliorini L, Molinaroli L, Simonetti R, Manzolini G. Development and experimental validation of a comprehensive thermoelectric dynamic model of photovoltaic modules. Solar Energy 2017;144:489–501.

[19] Osma-Pinto G, Ordóñez-Plata G. Dynamic thermal modelling for the prediction of the operating temperature of a PV panel with an integrated cooling system. Renewable Energy 2020;152:1041–1054.

[20] Diamant RME. Insulation Deskbook. Heating & Ventilating Publications Croydon; 1977.

[21] Bevilacqua P, Perrella S, Bruno R, Arcuri N. An accurate thermal model for the PV electric generation prediction: long-term validation in different climatic conditions. Renewable Energy 2021;163:1092–1112.

[22] Bevilacqua P, Bruno R, Rollo A, Ferraro V. A novel thermal model for PV panels with back surface spray cooling. Energy 2022;255:124401.

[23] Berdahl P, Martin M. Emissivity of clear skies. Solar Energy 1982;32(5):663–664.

[24] Prilliman M, Stein JS, Riley D, Tamizhmani G. Transient Weighted Moving-Average Model of Photovoltaic Module Back-Surface Temperature. IEEE Journal of Photovoltaics 2020;10(4):1053–1060.

[25] Evangelisti L, Guattari C, Asdrubali F. On the sky temperature models and their influence on buildings energy performance : A critical review. Energy & Buildings 2019;183:607–625.

[26] Albatayneh A, Alterman D, Page A, Moghtaderi B. The significance of sky temperature in the assessment of the thermal performance of buildings. Applied Sciences (Switzerland) 2020 11;10(22):1–16.

[27] Karn A, Chintala V, Kumar S. An investigation into sky temperature estimation, its variation, and significance in heat transfer calculations of solar cookers. Heat Transfer - Asian Research 2019;48(5):1830–1856.

[28] Korniyenko SV. The influence of the sky radiative temperature on the building energy performance. Magazine of Civil Engineering 2022;114(6).

[29] Ficker T. Are the local sky temperature models and the global thermal standard model EN ISO 6946(2017) numerically compatible? Indoor and Built Environment 2024;33(3):422–434.

[30] De Cristo E, Evangelisti L, Guattari C, De Lieto Vollaro R. An Experimental Direct Model for the Sky Temperature Evaluation in the Mediterranean Area: A Preliminary Investigation. Energies 2024;17(9):1–15.

[31] Pereira S, Canhoto P, Oozeki T, Salgado R. Assessment of thermal modeling of photovoltaic panels for predicting power generation using only manufacturer data. Energy Reports 2024;12:1431–1448.

[32] Liu J, Li X, Yang Y, Wu Y. Advancing PV temperature modeling: comparative evaluation and a novel empirical model. Applied Thermal Engineering 2026;291:130228.

[33] Ahmad W, D'Angola A, Malgaroli G, Spertino F, Ciocia A, Shahzad N. Comprehensive Analysis of Thermal-Electrical Models for PV Module: A Review of Current Approaches and Challenges. Energies 2026;19(5):1179.

[34] Driesse A, Theristis M, Stein JS. Improving Common PV Module Temperature Models by Incorporating Radiative Losses to the Sky. Sandia National Laboratories; 2022.

[35] Aoun N. Methodology for predicting the PV module temperature based on actual and estimated weather data. Energy Conversion and Management: X 2022;14:100182.

[36] Hassan MA, Bailek N, Bouchouicha K, Ibrahim A, Jamil B, Kuriqi A, et al. Evaluation of energy extraction of PV systems affected by environmental factors under real outdoor conditions. Theoretical and Applied Climatology 2022;150(1-2):715–729.

[37] Khyani HK, Vajpai J, Karwa R, Bhadu M. Thermal Modeling of Photovoltaic Panel for Cell Temperature and Power Output Predictions under Outdoor Climatic Conditions of Jodhpur. Journal of Electrical and Computer Engineering 2023;2023.

[38] Pereira S, Canhoto P, Oozeki T, Salgado R. Comprehensive approach to photovoltaic power forecasting using numerical weather prediction data and physics-based models and data-driven techniques. Renewable Energy 2025;251:123495.

[39] Li P, Luo Y, Xia X, Gao X, Chang R, Li Z, et al. Factors and quantitative impact on electrical yield in fishery complementary photovoltaic power plant under different cloud cover conditions. Energy 2024;309:133079.

[40] Correa-Betanzo C, Calleja H, De Leon-Aldaco S. Module temperature models assessment of photovoltaic seasonal energy yield. Sustainable Energy Technologies and Assessments 2018;27:9–16.

[41] Zhang K, P McDowell T, Kummert M. Sky Temperature Estimation and Measurement for Longwave Radiation Calculation. Building Simulation Conference Proceedings 2017;.

[42] Rabadiya A, Kirar R. Comparative Analysis of Wind Loss Coefficient (Wind Heat Transfer Coefficient) For Solar Flat Plate Collector. vol 2012;2:6. https://api.semanticscholar.org/CorpusID:110194368.

[43] Mattei M, Notton G, Cristofari C, Muselli M, Poggi P. Calculation of the polycrystalline PV module temperature using a simple method of energy balance. Renewable Energy 2006 4;31:553–567.

[44] Sánchez Barroso JC, Barth N, Correia JPM, Ahzi S, Khaleel MA. A computational analysis of coupled thermal and electrical behavior of PV panels. Solar Energy Materials and Solar Cells 2016;148:73–86.

[45] Torres Lobera D, Valkealahti S. Dynamic thermal model of solar PV systems under varying climatic conditions. Solar Energy 2013;93:183–194.

[46] Villemin T, Claverie R, Sawicki JP, Parent G. Thermal characterization of a photovoltaic panel under controlled conditions. Renewable Energy 2022;198:28–40.

[47] Garcia-Gutierrez L, Aillerie M, Sawicki JP, Zheng Z, Claverie R. Evaluation of solar photovoltaic efficiency on green and flat roofs: Experimental and comprehensive numerical analysis. Solar Energy 2024 8;278:112750.